Preferential targeting of lateral entorhinal inputs onto newly integrated granule cells

Nicholas I. Woods[1,2,*], Christopher E. Vaaga[1,*], Christina Chatzi[1], Jaimie D. Adelson[1], Matthew F. Collie[1], Julia V. Perederiy[1], Kenneth R. Tovar[1], Gary L. Westbrook[1]

1. Vollum Institute, Oregon Health and Science University, 3181 SW Sam Jackson Park Road, Portland OR, 97239, USA
2. Current Address: Medical Scientist Training Program, University of California San Francisco, San Francisco CA, 94143, USA

* These authors equally contributed to this work.

Corresponding Author:
Gary L. Westbrook
Vollum Institute, L474
Oregon Health and Science University
3181 SW Sam Jackson Park Road
Portland OR, 97008
westbroo@ohsu.edu

Keywords:
Dentate gyrus, pattern separation, tetanus toxin, optogenetics, retroviral labeling, synapse formation, Neurogenesis

Running title: Preferential targeting of newly integrated neurons

Acknowledgements: This work was supported by R01 NS080979 and the Ellison Medical Foundation (GLW) and P30 NS061800. We thank Stefanie Kaech Petrie for help with imaging. Thanks to Eric Schnell for guidance with electrophysiology. We thank Sue Aicher for assistance with electron microscopy.

Abstract:
Mature dentate granule cells in the hippocampus receive input from the entorhinal cortex via the perforant path in precisely arranged lamina, with medial entorhinal axons innervating the middle molecular layer and lateral entorhinal cortex axons innervating the outer molecular layer. Although vastly outnumbered by mature granule cells, adult-generated newborn granule cells play a unique role in hippocampal function, which has largely been attributed to their enhanced excitability and plasticity (Schmidt-Hieber et al., 2004; Ge et al., 2007). Inputs from the medial and lateral entorhinal cortex carry different informational content, thus the distribution of inputs onto newly integrated granules will affect their function in the circuit. Therefore we examined the functional innervation and synaptic maturation of newly-generated dentate granule cells using retroviral labeling in combination with selective optogenetic activation of medial or lateral entorhinal inputs. Our results indicate that lateral entorhinal inputs provide nearly all the functional innervation of newly integrated granule cells. Despite preferential functional targeting, the dendritic spine density of immature granule cells was not increased in the outer molecular layer compared to the middle molecular layer. However, chronic blockade of neurotransmitter release in medial entorhinal axons with tetanus toxin disrupted normal synapse development from both medial and lateral entorhinal inputs. Our results support a role for preferential lateral perforant path input onto newly generated neurons in mediating pattern separation, but also indicates that medial perforant path input is necessary for normal synaptic development.

Significance Statement: The formation of episodic memories involves the integration of contextual and spatial information. Newly integrated neurons in the dentate gyrus of the hippocampus play a critical role in this process, despite constituting only a minor fraction of total granule cells. Here we demonstrate that these neurons preferentially receive information thought to convey the context of an experience - a unique role that each newly integrated granule cell serves for about a month before reaching maturity.

63 **Introduction:**

64 As the entry point to the trisynaptic hippocampal circuit, the dentate gyrus has several
65 interesting features including a 'sparse' network design (Boss et al., 1985; Rolls et al., 1998),
66 laminated inputs carrying distinct informational content (Witter, 2007; Knierim et al., 2014), and
67 participation of mature granule cells alongside the continuous integration of newly-generated
68 neurons (Overstreet-Wadiche and Westbrook, 2006; Ming and Song, 2011). Hippocampal
69 granule cells receive highly laminar inputs from entorhinal cortex within the molecular layer of
70 the dentate gyrus. Input from medial entorhinal cortex, conveying spatial cues, is restricted to
71 the middle molecular layer (Ferbinteanu et al., 1999; Hafting et al., 2005; Hargreaves et al.,
72 2005; Yasuda and Mayford, 2006; Witter, 2007; Van Cauter et al., 2013), whereas input from
73 lateral entorhinal cortex conveying contextual information is restricted to the outer molecular
74 layer (Hargreaves et al., 2005; Hunsaker et al., 2007; Witter, 2007; Deshmukh and Knierim,
75 2011; Yoganarasimha et al., 2011; Tsao et al., 2013). Despite being substantially outnumbered
76 by mature granule cells, newly integrated granule cells are thought to uniquely contribute to
77 pattern separation (Clelland et al., 2009; Sahay et al., 2011; Nakashiba et al., 2012; Tronel et
78 al., 2012) - that is, the ability to distinguish between subtly different contexts - one of the primary
79 functions of the dentate gyrus (Deng et al., 2010; Aimone et al., 2011). This unique function
80 must occur during a narrow time window between initial integration into the perforant path circuit
81 (~3 weeks post-mitosis) and complete maturation of synapses (>8 weeks) (van Praag et al.,
82 2002; Ambrogini et al., 2004; Overstreet et al., 2004; Overstreet-Wadiche et al., 2006; Zhao et
83 al., 2006; Brunner et al., 2014).

84

85 The search for unique functions of newly integrated neurons has largely focused on intrinsic
86 properties, such as enhanced excitability and plasticity (Schmidt-Hieber et al., 2004; Abrous et
87 al., 2005; Ge et al., 2007; Marín-Burgin et al., 2012; Dieni et al., 2013). However, newborn
88 neurons also undergo rapid changes in connectivity, which differs from synapse remodeling in
89 early development (Goodman and Shatz, 1993; Katz and Shatz, 1996; Walsh and Lichtman,
90 2003), as newborn neurons integrate into an already established circuit (Toni et al., 2007,
91 2008), and compete for synaptic innervation with pre-existing axons of the perforant path.
92 Rabies-based circuit mapping suggests that inputs to newly integrated neurons may differ from
93 mature granule cells (Vivar et al., 2012).

94

95 Here, we directly assayed synaptic integration of newborn granule cells over the course of
96 excitatory synapse development using retroviral labeling of newborn neurons and laminar-

specific optogenetic stimulation of entorhinal inputs. Our results indicate that newly integrated granule cells preferentially receive functional synaptic input from lateral entorhinal cortex, whereas mature granule cells receive balanced input from medial and lateral entorhinal cortex. Although medial perforant path input was weak in newly integrated granule cells, chronic silencing of this pathway using tetanus toxin impaired the functional and morphological development of lateral perforant path inputs.

Methods:

Animals: We used male and female C57/Bl6 mice. Animal procedures were carried out in accordance with the Oregon Health and Science University Institutional Animal Care and Use Committee, Biosafety Committee protocols, and NIH guidelines for the safe handling of animals.

Viral Constructs: To selectively transfect and visualize adult-born hippocampal granule cells, we used a replication-deficient Moloney Murine Leukemia Virus-based retroviral vector that requires cell mitosis for transduction (Luikart et al., 2011). The retrovirus contained an internal ubiquitin 6 promoter that drives expression of GFP (viral titer 10^5) as described previously (Luikart et al., 2011). To express the light-activated ion channel channelrhodopsin-2 (ChR2) selectively in entorhinal cortex axons projecting to the middle or outer molecular layer, we stereotaxically injected an AAV9-CAG-ChR2-eGFP viral construct (UNC Viral Core) into the medial or lateral entorhinal cortex. To selectively silence axons, we injected a custom AAV-CAG-TeNT-mCherry virus (viral titer 10^{13}) made by cloning a 2kb fragment encoding the light chain of tetanus toxin fused with mCherry into an AAV backbone using InFusion cloning. AAV vectors were serotyped with AAV9 coat proteins and packaged at the University of North Carolina Vector Core.

Stereotaxic Injections: Stereotaxic viral injections into 6-8 week old male and female C57/Bl6 mice were carried out using a Model 1900 Stereotaxic Alignment System (Kopf). Mice were anesthetized with 2% isoflurane, and a small incision was created over the skull following application of artificial tears to the eyes and antibiotic/iodine around the incision site. A Model 1911 Stereotaxic Drill was used to create burr holes over the injection site. pRubi-GFP retrovirus to label mitotically active granule cells was injected into the dentate gyrus (coordinates: in mm from bregma): anteroposterior: -1.9, lateromedial: +/- 1.1; dorsoventral: -2.5, -2.3. One microliter of non-diluted virus was injected at 250 nl/min with a 10 µl Hamilton syringe fitted with a 30-gauge needle using a Quintessential stereotaxic injector (Stoetling).

131 After each injection, the needle was left in place for 1 minute to allow for diffusion of the virus
132 and prevent backflow. Injections of AAV9-CAG-CHR2-GFP into the lateral entorhinal cortex
133 were made at anteroposterior: -3.4, lateromedial: +/- 4.0; dorsoventral: -2.4. Injections of AAV9-
134 CAG-ChR2-GFP or AAV9-CAG-TeNT-mCherry into the medial entorhinal cortex were made at
135 anteroposterior: -4.5; dorsoventral: +/- 3.0; dorsoventral: -3.2. Following injection, mice received
136 topical lidocaine and drinking water with cherry-flavored Tylenol, and monitored every 24 hours
137 over 3 days.
138
139 *Immunohistochemistry and Spine Counts:* Mice were transcardially perfused with ice-cold 4%
140 sucrose in 0.1 M PBS followed by fixative containing 4% sucrose and 4% paraformaldehyde
141 (PFA) in PBS. Brains were removed, and postfixed (4% PFA, 1x PBS) overnight at 4ºC. The
142 dorsal hippocampus was sectioned (coronal, 100 µm) using a Leica VT 1000s vibratome.
143 Sections were permeabilized with 0.4% Triton X-100 in PBS (PBS-T), blocked with filtered 10%
144 horse serum in PBS-T and incubated in primary antibody overnight in 1.5% horse serum in
145 PBS-T. Primary antibodies included: 1:300 Alexa-Fluor 488-conjugated rabbit anti-GFP (catalog
146 no. A21311, Invitrogen), 1:500 anti-VGlut2 (catalog no. 135 404, Synaptic Systems), and 1:500
147 anti-glial associated fibrillary protein (GFAP; catalog no. Z-0334, DAKO). Sections were then
148 rinsed with PBS-T and incubated for 2-3 hours at room temperature in PBS-T with secondary
149 antibodies: 1:300 Alexa Fluor 488-conjugated anti-GFP (A21311, Invitrogen), 1:200 goat anti-
150 guinea pig Alexa Fluor 568 (A11075, Invitrogen), 1:200 goat anti-rabbit Alexa Fluor 488). The
151 mCherry-TeNT signal was visualized using native fluorescence**.** The tissue was counterstained
152 with DAPI using Fluoromount G with DAPI (SouthernBiotech).
153
154 Images were acquired using either a Zeiss LSM 770 or LSM 780 laser-scanning confocal
155 microscope on a motorized AxioObserver Z1 inverted scope (Carl Zeiss MicroImaging).
156 Dendrites for spinal analysis were imaged using a 63x objective (1.4 NA, oil, 2x zoom). For each
157 imaged cell, dendritic segments in the middle molecular layer and the outer molecular layer
158 were imaged. The middle and outer molecular layer were distinguished based on VGluT2
159 immunofluorescence pattern, which begins at the border between the inner molecular layer and
160 middle molecular layer. Middle molecular layer dendritic segments were therefore imaged at the
161 beginning of the VGluT2 staining, whereas outer molecular layer dendritic segments were
162 imaged at the distal tip of the molecular layer. Spine density analysis was performed blinded to
163 experimental condition. The Cell Counter plugin in FIJI (NIH) was used to count and categorize
164 spines (Harris et al., 1992), and Simple Neurite Tracer (FIJI) was used to measure dendritic

165 segment length. Spine density and spine type between the middle and outer molecular layer
166 was compared across conditions (control and TeNT overexpression) and developmental time
167 points (3-12 weeks post-viral injection). Spine morphology was visually assessed: dendritic
168 spines containing a spine head (ca. 2x shaft diameter) were considered as mushroom spines
169 and all other spines were considered filopodia-like.
170
171 *Electrophysiology:* Electrophysiological recordings were made 21 days after viral injection to
172 allow for construct expression. Acute coronal brain slices were prepared as described
173 previously (Perederiy et al., 2013). Briefly, animals were anesthetized with an intraperitoneal
174 injection of 2% 2,2,2-tribromoethanol (0.7-0.8 mL), and transcardially perfused with an ice-cold,
175 oxygenated modified ACSF which contained (in mM): 110 choline-Cl, 7 MgCl2, 2.5 KCl, 1.25
176 NaH2PO4, 0.5 CaCl, 1.3 Na-ascorbate, and 25 NaHCO3. Hippocampi were resected and cut at
177 300 µm in the transverse axis on a Leica 1200s vibratome. Slices were allowed to incubate for 1
178 hr in 37ºC normal ACSF, which contained (in mM): 125 NaCl, 2.5 KCl, 2.0 CaCl, 1.0 MgCl2,
179 1.25 NaH2PO4, 25 NaHCO3, and 25 glucose.
180
181 We used glass pipettes (2-3 MΩ) filled with normal ACSF for extracellular field recording, which
182 were placed into the lamina of interest. Presynaptic fibers were stimulated using a bipolar
183 electrode (3-7v, 0.5v steps) or optogenetic stimulation (1ms pulses of 470 nm blue light). Whole-
184 cell voltage clamp recordings were made using glass pipettes (5-8 MΩ). Mature granule cells
185 were selected based on input resistance less than 750 MΩ (495±37 MΩ) and soma position in
186 the outer ⅓ of the granule cell layer (Ambrogini et al., 2004; Overstreet-Wadiche and
187 Westbrook, 2006). The whole-cell recording solution contained (in mM): 100 gluconic acid, 0.2
188 EGTA, 5 HEPES, 2 Mg-ATP, 0.3 Li-GTP (pH: 7.2, 295 mOsm; adjusted with 50% CsOH such
189 that final concentration of Cs-gluconate is 100-120 mM). The liquid junction potential (- 7 mV)
190 was not corrected. Input resistance of the cell was continually monitored with a 10 mV
191 hyperpolarizing step, and cells with input resistance exceeding 25 MΩ at any point were
192 excluded from analysis. Data was acquired at 10 KHz and Bessel filtered at 4 KHz on a
193 Multiclamp 700B (Axon Instruments, Sunnyvale CA) and recorded using AxographX acquisition
194 software (www.axograph.com).
195
196 Optogenetic stimulation was provided by an 470 nm LED (ThorLabs, Newton, NJ). Light pulses
197 (1 ms) were provided through the microscope objective, which was centered over the
198 appropriate lamina. Optical stimulation was provided over a range of intensities until a maximal

199 response was elicited, which was then used for the remainder of the experiment. Peak EPSC
200 amplitudes were measured using a built-in routine in AxographX. Miniature EPSCs were
201 recorded in the presence of SR95531 (10 μM) and TTX (1 μM) to isolate miniature excitatory
202 events. Quantal events were detected using a sliding window template consisting of a single
203 exponential (-10 pA, 1 ms rise time, 6 ms decay time constant). Individual events were then
204 manually inspected. mEPSC analysis was performed with the experimenter blinded to condition.
205
206 *Cell Culture:* Mouse hippocampal neurons were cultured on glial micro-islands as described
207 previously (Tovar et al., 2009). Briefly, neonatal (postnatal day 0-1) male mice were
208 decapitated, and the hippocampi were dissected. Micro-islands were generated by plating at
209 125,000 cells/35 mm dish. After 7 days *in vitro*, cultures were treated with 200 μM glutamate for
210 30 min to kill any neurons. Neurons were then plated on the remaining glial feeder layer at
211 25,000 cells/35 mm dish and maintained in a tissue culture incubator (37ºC, 5% CO_2) until use.
212 The culture medium consisted of minimum essential media with 2 mM glutaMAX (Invitrogen),
213 5% heat-inactivated fetal calf serum (Lonza), and 1 ml/l MITO+ Serum Extender (BD
214 Biosciences). The culture medium was supplemented with glucose to a final concentration of 21
215 mM. Cultured neurons were transduced at 1 day *in vitro* by replacing 50% of the culture medium
216 with virus-containing medium (1 μL of virus in 500 μL medium). After 24 hours, the virus-
217 containing medium was removed and replaced with fresh complete medium.
218
219 Whole cell voltage clamp recordings were made from cultured neurons 3-16 days *in vitro*. The
220 extracellular recording solution consisted of (in mM): 158 NaCl, 2.4 KCl, 1.3 $CaCl_2$, 1 $MgCl_2$, 10
221 HEPES and 10 D-glucose (pH 7.4; 320 mosmol). Glass pipettes (2-6 MΩ) were filled with a
222 solution which contained (in mM): 140 K-gluconate, 4 $CaCl_2$, 8 Na Cl, 2 $MgCl_2$, 10 EGTA, 10
223 HEPES, 4 Na_2ATP and 0.2 Na_2GTP (pH: 7.4, 319 mosmol). Autaptic EPSCs were elicited from
224 neurons in isolation on a glial micro-island with a brief voltage command (+30 mV, 0.5 ms) to
225 elicit an unclamped action potential. Recordings were made in the presence of 10 μM SR95531
226 and 10 μM (R)-CPP to block $GABA_A$ and NMDA receptors, respectively. Data was acquired
227 using an Axopatch 1C amplifier and AxographX (www.axograph.com) acquisition software. In all
228 recordings, the series resistance was <10 MΩ and was continuously monitored with a -10 mV
229 step. Data was low-pass Bessel filtered at 4 kHz and sampled at 10 kHz.
230
231 *Electron Microscopy:* Ultrastructural analysis of control and TeNT expressing medial perforant
232 path axons was done 21-days post viral injection, as in Perederiy et al., 2013. Two control

233 (pRubi-expressing) and two pRubi and TeNT-expressing animals were transcardially perfused
234 with PBS followed by a 3.75% acrolein and 2% paraformaldehyde fixative. The brains were then
235 extracted and stored in 2% paraformaldehyde for at least 1 hour prior to sectioning at 40 μm in
236 the coronal plane using a Leica VT 1000s vibratome (Leica Microsystems). Sections including
237 the dorsal hippocampus were incubated in 1% sodium borohydride for 30 minutes to reduce
238 nonspecific binding, followed by incubation in 10% Triton-X for 45 minutes to increase antibody
239 penetration. Next, sections were blocked with 0.5% bovine serum albumin for 1 hour followed by
240 primary antibody incubation directed against pRubi-GFP (Rabbit α-GFP; 1:500, Millipore Cat #:
241 AB3080) or TeNT-mCherry (Mouse α-mCherry; 1-500, Living Colors Cat #: 632543) overnight at
242 4ºC. Following primary antibody incubation, the tissue was thoroughly washed with 0.4% Triton-
243 X. To visualize GFP, tissue was incubated in biotinylated goat α-rabbit secondary antibody
244 (1:200; Vector Laboratories, Cat # BA-1000) for 2 hours at room temperature followed by avidin-
245 binding complex (Vector Laboratories, Burlingame CA) for 30 minutes then reacted with DAB-
246 H_2O_2 solution for 5.5 minutes. To visualize mCherry, the tissue was incubated in goat α-mouse
247 gold-conjugated IgG (1:50; Aurion, Cat #: 800.422) for 2 hours at room temperature. Tissue was
248 then washed with citrate buffer and silver enhanced for 6.5 minutes.
249
250 Following DAB and/or immunogold reactions, the tissue was fixed in 1% osmium tetroxide for 15
251 minutes in 0.1 M phosphate buffer. Tissue was then washed and dehydrated through an ethanol
252 series before being incubated in propylene oxide (10 minutes) and propylene oxide:EMBed (1:1
253 solution) overnight. Finally, the tissue was embedded in Aclar resin and placed in an oven at
254 60ºC for 24 hours. 700 nm coronal sections were made using a Leica EM UC6 vibratome (Leica
255 Microsystems). Some sections were mounted on glass slides and stained with toluidine blue in
256 0.5 % sodium tetraborate to assist in region selection. Tissue from the supra-pyramidal blade of
257 the dentate gyrus was sectioned at 70 nm using an ultramicrotome (Leica Microsystems).
258 Sections were placed on 200 square mesh copper/rhodium grids and counterstained with 5%
259 uranyl acetate and Reynold's lead citrate. The middle molecular layer was imaged at 11,000x
260 on an FEI Technai G^2 12 BioTWIN microscope at 80 kV. At least 10 representative images were
261 selected in both control and TeNT expressing conditions.
262
263 *Experimental Design and Statistical Analysis:* Male and female mice were used for all
264 experiments except developmental spine analysis, in which only males were used to provide
265 more consistent results across animals. All data are reported as mean±SEM unless otherwise
266 noted. Statistical analysis was performed in Prism6 (GraphPad Software, La Jolla, CA). Data

267 were assumed to be normally distributed, in accordance with previous datasets in this circuit.
268 Spine density data were analyzed using a two-way repeated measures ANOVA (repeated
269 measures: days post-mitosis, lamina). Pooled data were analyzed using an ANOVA with Holm-
270 Sidak post-hoc analysis. Electrophysiology data were analyzed using two-tailed unpaired
271 Student's t-tests. Linear regressions were performed using an Extra-sum of squares F-test.
272 Sample sizes were chosen to detect an effect size of 20%, based on previous experiments, with
273 a power of 0.8. Statistical significance was defined as $\alpha<0.05$, and was adjusted for post-hoc
274 comparisons (Holm-Sidak), as appropriate.
275
276
277 **Results**
278 *Adult-born granule cells receive preferential input from outer molecular layer axons*
279 To examine the perforant path input onto newborn granule cells, we used electrical and
280 optogenetic laminar-specific stimulation (Figure 1 A). Targeting of the medial or lateral perforant
281 path was possible using a bipolar electrode as demonstrated by changes in the polarity of the
282 field EPSP (Figure 1 B, Andersen et al., 1966). However, optogenetic labeling allows more
283 precise pathway-specific stimulation. Thus we injected AAV9-CAG-ChR2-eGFP into either
284 medial or lateral entorhinal cortex, which provided very precise labeling of either the medial or
285 lateral perforant path fibers in the molecular layer (Figure 1C).
286
287 As expected, in mature cells, there was no difference in the maximal amplitude of light-evoked
288 EPSCs from the medial (MPP) or lateral perforant path (LPP) (MPP: 123.0±24.7 pA, n=19 cells;
289 LPP: 105.9±31.3 pA, n=16 cells; Student's unpaired t-test: t(33): 0.46, p=0.67 ; Figure 1 D, E),
290 indicating that mature cells receive robust and balanced excitatory input from both layers.
291 Surprisingly, in newly integrated neurons (retrovirally labeled cells, 21 days post-mitosis), the
292 strength of lateral perforant path inputs was nearly 10-fold larger than inputs from the medial
293 perforant path (MPP: 7.8±3.1 pA, n=14 cells; LPP: 72.2±15.2 pA, n=18 cells; Student's unpaired
294 t-test: t(30): 3.68, p=0.0009:; Figure 1 D, E). The reduced strength of medial perforant path
295 inputs in newly integrated granule cells was not a result of NMDA-only or 'silent' synapses, as
296 there was no difference in the AMPA/NMDA ratio between lamina (MPP: 5.2±1.3, n=13 cells;
297 LPP: 3.66±0.58, n=13 cells; Student's unpaired t-test: t(24): 1.04; p=0.31). These results
298 indicate that newly integrated neurons receive preferential, but not exclusive, functional input
299 from the lateral perforant path.
300

Synapse formation in newborn granule cells does not involve competitive elimination

Given the differences in synaptic strength between lateral and medial perforant path axons in newly integrated granule cells, we examined whether exuberant synapse formation occurs in the lateral perforant path, followed by competitive elimination and synaptic rebalancing, as seen during early development (Goodman and Shatz, 1993; Katz and Shatz, 1996; Walsh and Lichtman, 2003). We labeled mitotically active neurons in 6 week-old male mice with a retroviral pRUBI-GFP vector (Luikart et al. 2012), then examined spine density in 3 to 12 week-old cells (at 1 week intervals) in the middle molecular layer (MML) and outer molecular layer (OML). Despite the functional difference in synapse strength in newly integrated granule cells, there was no difference in spine density across laminae at any time point (two-way repeated measure ANOVA: $F(1,2)$: 0.195, $p=0.7$). In grouped data from both laminae, the spine density increased from 3 to 4 weeks post-injection (3 wk: 0.98±0.07 spines/μm, n=36 dendritic segments from 3 animals; 4 wk: 1.52±0.03 spines/μm, n=36 dendritic segments from 3 animals; Holm-Sidak post-hoc comparison: $t(47)$: 4.5, $p<0.001$; Figure 2 A, B), but then remained unchanged between 4 and 12 weeks post-injection (Holm-Sidak post-hoc comparison: $p>0.05$). The spine density at 12 weeks is within the range of reported values for mature granule cells (Parent et al., 2016).

The morphology of dendritic spines also changed during this time period, as there was an increase in the proportion of spines with filopodial morphology in the middle molecular layer (3 wk: 13.3±1.3% of total spines, n=14 cells; 6 wk: 23.21±2.6% of total spines, n=16 cells; Student's unpaired t-test: $t(28)$: 3.29, $p=0.0027$; Figure 2 A, C) and outer molecular layer (3 wk: 12.53±2.3% of total spines, n=10 cells; 6 wk: 25.42±2.6% of total spines, n=13 cells; Student's unpaired t-test: $t(21)$: 3.54, $p=0.002$; Figure 2 A, C). In contrast to spine density, the mEPSC frequency remained unchanged between 3 and 6 weeks post mitosis (3 wk: 0.08±0.02 Hz, n=15 cells, 6 wk: 0.05±0.01 Hz, n=10 cells; Student's unpaired t-test: $t(23)$: 1.32, $p=0.20$; Figure 2 D, E). At 6 weeks post mitosis, there was a small decrease in the mESPC amplitude (3 wk: 16.2±0.8 pA, n=15 cells; 6 wk: 13.5±1.0 pA, n= 10 cells, Student's unpaired t-test: $t(23)$: 2.1, $p=0.045$, Figure 2 D, F), perhaps consistent with the observed increase in filopodial spines (Holtmaat and Svoboda, 2009). This data suggests that during this period of functional synaptic rebalancing, synapse formation by newly integrating granule cells does not involve over-abundant synapse formation followed by synaptic pruning.

335 *Chronic silencing with TeNT*

336 To chronically silence axonal input in a laminar-specific manner, we virally expressed tetanus
337 toxin light chain (TeNT), which cleaves the SNARE complex protein synaptobrevin-2, thereby
338 preventing neurotransmitter release (Schiavo et al., 1992). We chose to use tetanus toxin
339 because it has the advantage of completely silencing axons, with the disadvantage that effects
340 are irreversible. As the degree of silencing may influence effects on excitatory synapse
341 formation (Bagley and Westbrook, 2012), we carefully validated our tetanus toxin vector *in vitro*
342 and *in vivo*. First, we examined AMPA receptor currents in neurons in autaptic cultures (Tovar et
343 al., 2009). In control cells an unclamped action potential at the soma elicited a large amplitude,
344 NBQX-sensitive EPSC without failure (n=7 cells; Figure 3 A, B). However, expression of TeNT
345 by viral transfection completely abolished EPSCs (EPSC success rate: 0.22±0.2%, n=10 cells,
346 Student's unpaired t-test: t(14): 392.9 p<0.0001; Figure 3 A, B).
347
348 To selectively silence medial perforant path inputs *in vivo*, we injected an AAV9-TeNT-mCherry
349 virus into the medial entorhinal cortex (Figure 3 C), resulting in robust laminar-specific
350 expression of TeNT in medial perforant path axons (Figure 3 C, D). TeNT expression was
351 accompanied by a lamina-specific decrease in VGluT1 immunostaining, a marker of functional
352 presynaptic terminals (Figure 3 D). Importantly, TeNT expression followed up to 6 weeks *in vivo*
353 did not elicit an inflammatory response (Figure 3 E), unlike the glial scarring that occurs
354 following axotomy of medial perforant path axons with subsequent degeneration of terminal
355 axons (Perederiy et al., 2013). Immunogold electron micrographs of TeNT-expressing axon
356 terminals had pronounced swelling as well as increased accumulation of small clear vesicles in
357 presynaptic boutons, consistent with complete block of vesicular release (Figure 3 F, G). TeNT-
358 expressing axon terminals were directly apposed to dendritic spines, further suggesting that
359 TeNT-expression did not elicit axon degeneration.
360
361 To examine the efficiency of silencing of the middle molecular layer, we recorded fEPSP
362 responses to laminar-specific medial perforant path electrical stimulation in control and TeNT-
363 expressing slices. Consistent with our *in vitro* results, TeNT markedly reduced the maximal
364 fEPSP slope (control: 0.67±0.07 μV/ms, n=6 slices; TeNT: 0.26±0.02 μV/ms, n=5 slices;
365 Student's unpaired t-test: t(9): 5.4, p=0.0004; Figure 3 H), as well as the input-output
366 relationship between fiber volley amplitude and fEPSP slope (control: 0.52±0.003; TeNT:
367 0.24±0.01; Extra Sum of Squares F-test: F(1,105): 30.4, p<0.0001; Figure 3 I). Importantly,
368 there was no difference in the fiber volley amplitude with maximal stimulation (control: -

369 231.7±36.5 μV, n=5 slices; TeNT: -197±29.8 μV, n=5 slices; Student's unpaired t-test: t(8): 0.74,
370 p=0.48), indicating that equal numbers of axons were stimulated in both conditions. The small
371 residual fEPSP response observed in slices likely indicates that a few medial entorhinal cortex
372 neurons had not been infected with TeNT.
373
374 *Silencing the middle molecular layer impairs synapse formation with perforant path inputs.*
375 Although the medial perforant path provides only weak input onto newly integrated granule cells,
376 dendritic spines are present, and thus these inputs could have an activity-dependent effect on
377 circuit formation. We used laminar-specific silencing with TeNT to address this issue. ChR2-
378 eGFP was expressed in lateral perforant path axons in conjunction with TeNT-mCherry
379 expression in the medial perforant path (MPP:TeNT) (Figure 4 A). Interestingly, expression of
380 TeNT in the medial perforant path reduced the amplitude of lateral perforant path responses in
381 newly integrated granule cells (control: 72.2±15.2 pA, n=18 cells; MPP:TeNT:8.7±3.7 pA, n=8
382 cells; Student's unpaired t-test: t(24): 2.7, p=0.011; Figure 4 B, C), but not in mature granule
383 cells (control: 105.9±31.3 pA, n=16 cells; MPP:TeNT: 125.7±23.24 pA, n=23 cells; Student's
384 unpaired t-test: t(37): 0.52, p=0.6; Figure 4 B, C). There was also an increase in the paired
385 pulse ratio of lateral perforant path axons targeting newly integrated granule cells (control PPR:
386 0.9±0.08, n= 18 cells, MPP:TeNT PPR: 1.8±0.3, n=8 cells; Student's unpaired t-test: t(24): 4.3,
387 p=0.0003; Figure 4 B, D). This change was not observed in mature granule cells (control PPR:
388 1.1±0.07, n= 16 cells; MPP:TeNT PPR: 1.4±0.2, n=23 cells, Student's unpaired t-test: t(37):
389 1.38, p=0.17; Figure 4 B, D).
390
391 Silencing of the medial perforant path also reduced the spine density of newly integrated
392 granule cells in both the middle molecular layer (control: 0.95±0.04 spines/μm, n=24 dendritic
393 segments from 4 animals; MPP:TeNT: 0.51±0.05 spines/μm, n=24 dendritic segments from 4
394 animals; Student's unpaired t-test: t(6): 7.12, p=0.0004; Figure 4 F, G) and outer molecular layer
395 (control: 0.93±0.03 spines/μm, n=24 dendritic segments from 4 animals; MPP:TeNT: 0.54±0.02
396 spines/μm, n=24 dendritic segments from 4 animals; Student's unpaired t-test: t(6): 11.01,
397 p<0.0001; Figure 4 F, G). Together these results suggest that although the axons of the medial
398 perforant path make little contribution to the synaptic activation of adult-born granule cells, intact
399 synaptic release from medial perforant path axons is required for proper functional synaptic
400 integration of adult-born granule cells.
401
402

403 **Discussion**

404 There is general consensus that newborn neurons, once they integrate into the dentate gyrus
405 network, have a unique role in memory formation (Aimone et al., 2006; Saxe et al., 2006; Kee et
406 al., 2007). Newborn neurons go through a relatively stereotyped maturation post-mitosis,
407 including early GABAergic depolarization without excitatory perforant input for several weeks
408 (Ge et al., 2006) as their dendrites extend through the molecular layer (Zhao et al., 2006) . Prior
409 results have suggested a contribution of enhanced excitability and synaptic plasticity as a
410 reason that such a minor population can have a major impact on circuit function (Schmidt-
411 Hieber et al., 2004; Aimone et al., 2011). However, monosynaptic labeling studies using
412 modified rabies virus (Vivar et al., 2012) suggest that newborn neurons may have distinct
413 connectivity as well, with extrinsic excitatory input onto newborn neurons originating primarily
414 from the lateral entorhinal cortex. Our results indicate that newly integrated neurons receive
415 preferential functional input from the lateral entorhinal cortex, which likely contributes to their
416 role in pattern separation. Yet our data also show that preferential targeting must occur during a
417 well-defined time window followed by functional synaptic reorganization that results in balanced
418 input from medial and lateral entorhinal cortex.

419

420 *The preferential input onto newly generated granule cells*

421 Episodic memory requires both spatial and non-spatial information, which are differentially
422 encoded in medial and lateral entorhinal cortex, respectively (Ferbinteanu et al., 1999; Hafting
423 et al., 2005; Hargreaves et al., 2005; Yasuda and Mayford, 2006; Hunsaker et al., 2007;
424 Deshmukh and Knierim, 2011; Yoganarasimha et al., 2011; Tsao et al., 2013; Van Cauter et al.,
425 2013). Thus the strict laminar organization in the molecular layer provides a framework in which
426 distinct populations of granule cells or different regions of the dendritic tree, proximal vs distal,
427 may differentially affect circuit function (Magee, 2000; Dieni et al., 2013, 2016). In this setting,
428 the combination of the observed preferential functional targeting of lateral entorhinal cortex
429 inputs onto newly integrated granule cells complements their well-documented enhanced
430 plasticity (Schmidt-Hieber et al., 2004; Abrous et al., 2005; Ge et al., 2007) in mediating distinct
431 aspects of memory formation (Clelland et al., 2009; Sahay et al., 2011; Nakashiba et al., 2012;
432 Tronel et al., 2012). For example, this may fit with the role of newly integrated neurons as
433 novelty detectors for incoming contextual information, the essence of pattern separation (Deng
434 et al., 2010; Aimone et al., 2011). The preferential input from lateral entorhinal cortex indicates
435 that information processing in newly integrated neurons is functionally distinct from mature
436 neurons. Although the specific information carried by the lateral and medial perforant path is

437 likely to be more complex than a simple segregation of spatial and contextual input (Knierim et
438 al., 2014), the strict anatomical lamination of the molecular layer suggests that the two inputs
439 remain segregated along the dendritic tree of granule cells.
440
441 Despite the weak input from the medial perforant path, in our experiments there was no
442 difference in spine density on newly integrated granule cells between middle and outer
443 molecular layers. At the synaptic level, the preferential functional input could not be attributed to
444 an increase in 'silent synapses' (Isaac et al., 1995; Carroll and Malenka, 2000; Ziv and Garner,
445 2001; Feldman, 2009), as there was no difference in the AMPA/NMDA ratio between medial
446 and lateral perforant path inputs. Perhaps surprisingly, the presence of the same density of
447 spines within the middle molecular layer indicates spine morphology is dissociated from
448 functional synaptic strength in newly generated granule cells. Although presynaptic axon
449 terminals generally co-localize with postsynaptic spines, spine formation can be temporally
450 distinct from functional synapse formation (Yuste and Bonhoeffer, 2004). In fact, following
451 lesions of the perforant path, newly integrated granule cells continue to form dendritic spines
452 despite the loss of presynaptic axon terminals (Perederiy et al., 2013; see also Sando et al.,
453 2017). Furthermore, excitatory synapses may initially form on dendritic shafts as opposed to
454 spines (Crain et al., 1973; Miller and Peters, 1981; Mates and Lund, 1983; Yuste and
455 Bonhoeffer, 2004; Fortin et al., 2014), which may explain why the mEPSC frequency did not
456 increase between 3 and 6 weeks post-mitosis in our experiments.
457
458 *The role of the medial perforant path*
459 Our results indicate medial perforant path inputs are necessary for normal synapse formation of
460 all perforant path inputs on newly integrated granule cells. Adult-born granule cells in the
461 hippocampus share many properties with immature neurons during development (Schmidt-
462 Hieber et al., 2004; Abrous et al., 2005; Ge et al., 2007), but are unique in that they must
463 integrate into a pre-existing circuit (Ge et al., 2007; Toni et al., 2007; Adlaf et al., 2017). The
464 preferential functional targeting by the lateral entorhinal cortex is somewhat surprising from a
465 developmental perspective given that as newborn cells mature, their dendrites first pass through
466 the middle molecular layer, which is occupied by axons innervating mature granule cells. Inputs
467 from the medial entorhinal cortex were weak in newly integrated neurons, perhaps explaining
468 why it was not detected in rabies tracing studies of 21 days post-mitosis granule cells (Vivar et
469 al., 2012). However, chronic silencing of medial perforant path inputs with tetanus toxin nearly
470 eliminated the strong input from the lateral entorhinal cortex without affecting the lamination of

471 incoming axons. The effect of silencing was selective for inputs onto newly generated neurons
472 and occurred even though not every axon in the medial perforant path expressed tetanus, as
473 estimated from the residual field EPSP. Silencing the medial perforant path was accompanied
474 by a reduction in spine density in both the middle and outer molecular layer, although the
475 reduction in synaptic strength was greater than the reduction in spine density. Interestingly, this
476 pattern contrasts with homeostatic plasticity observed in some circuits (Davis, 2013). Given the
477 weak nature of this input, it may be that factors other than net neural activity contribute to the
478 developmental role of the medial perforant path inputs (i.e. neurotrophic factors; (Huang and
479 Reichardt, 2001; Cohen-Cory et al., 2010).
480
481 *Comparison to synapse formation during early development*
482 The existence of activity- and competition-dependent synapse remodeling is well mapped in the
483 immature brain as neural circuits first develop (Goodman and Shatz, 1993; Katz and Shatz,
484 1996; Walsh and Lichtman, 2003). In many developing brain circuits, neurons initially form an
485 overabundance of weak synapses which are later pruned in a competition-dependent manner,
486 resulting in the retention of strong synaptic inputs (Bear, 1995; Knudsen, 2004; Majewska and
487 Sur, 2006; Bhatt et al., 2009; Feldman, 2009). Such activity-dependent synaptic competition is
488 critical in the formation of mature, functional circuits (LeVay et al., 1980; Walsh and Lichtman,
489 2003; Datwani et al., 2009). These processes of synapse pruning and redistribution occur
490 during critical periods of development, when incoming patterns of activity strongly influence
491 circuit remodeling (Malenka and Bear, 2004; Holtmaat and Svoboda, 2009; Caroni et al., 2014).
492 However, in the adult brain, such circuit plasticity is more limited (Tagawa et al., 2005; Sato and
493 Stryker, 2008), suggesting that the basic pattern of initial synapse formation and subsequent
494 remodeling/refinement in adult-born cells may be distinct. Indeed we did not see a period of
495 synaptic overabundance as newly integrated cells reached maturity. Rather the period of
496 synaptic ‘competition’ for newly integrating neurons reflects a rebalancing of functional inputs
497 across the molecular layer. Remodeling in the adult environment is relevant not only to
498 neurogenic niches, but also to repair after neural injury or cell transplantation approaches
499 (Lindvall and Kokaia, 2006; Lepousez et al., 2015).
500
501
502
503
504

505 **References:**

506 Abrous DN, Koehl M, Le Moal M (2005) Adult neurogenesis: from precursors to network and
507 physiology. Physiol Rev 85:523–569.

508 Adlaf EW, Vaden RJ, Niver AJ, Manuel AF, Onyilo VC, Araujo MT, Dieni CV, Vo HT, King GD,
509 Wadiche JI, Overstreet-Wadiche L (2017) Adult-born neurons modify excitatory synaptic
510 transmission to existing neurons. Elife 6 Available at: http://dx.doi.org/10.7554/eLife.19886.

511 Aimone JB, Deng W, Gage FH (2011) Resolving new memories: a critical look at the dentate
512 gyrus, adult neurogenesis, and pattern separation. Neuron 70:589–596.

513 Aimone JB, Wiles J, Gage FH (2006) Potential role for adult neurogenesis in the encoding of
514 time in new memories. Nat Neurosci 9:723–727.

515 Ambrogini P, Lattanzi D, Ciuffoli S, Agostini D, Bertini L, Stocchi V, Santi S, Cuppini R (2004)
516 Morpho-functional characterization of neuronal cells at different stages of maturation in
517 granule cell layer of adult rat dentate gyrus. Brain Res 1017:21–31.

518 Bagley EE, Westbrook GL (2012) Short-term field stimulation mimics synaptic maturation of
519 hippocampal synapses. J Physiol 590:1641–1654.

520 Bear MF (1995) Mechanism for a sliding synaptic modification threshold. Neuron 15:1–4.

521 Bhatt DH, Zhang S, Gan W-B (2009) Dendritic spine dynamics. Annu Rev Physiol 71:261–282.

522 Boss BD, Peterson GM, Cowan WM (1985) On the number of neurons in the dentate gyrus of
523 the rat. Brain Res 338:144–150.

524 Brunner J, Neubrandt M, Van-Weert S, Andrási T, Kleine Borgmann FB, Jessberger S,
525 Szabadics J (2014) Adult-born granule cells mature through two functionally distinct states.
526 Elife 3:e03104.

527 Caroni P, Chowdhury A, Lahr M (2014) Synapse rearrangements upon learning: from divergent-
528 sparse connectivity to dedicated sub-circuits. Trends Neurosci 37:604–614.

529 Carroll RC, Malenka RC (2000) Delivering the goods to synapses. Nat Neurosci 3:1064–1066.

530 Clelland CD, Choi M, Romberg C, Clemenson GD Jr, Fragniere A, Tyers P, Jessberger S,
531 Saksida LM, Barker RA, Gage FH, Bussey TJ (2009) A functional role for adult
532 hippocampal neurogenesis in spatial pattern separation. Science 325:210–213.

533 Cohen-Cory S, Kidane AH, Shirkey NJ, Marshak S (2010) Brain-derived neurotrophic factor and
534 the development of structural neuronal connectivity. Dev Neurobiol 70:271–288.

535 Crain B, Cotman C, Taylor D, Lynch G (1973) A quantitative electron microscopic study of
536 synaptogenesis in the dentate gyrus of the rat. Brain Res 63:195–204.

537 Datwani A, McConnell MJ, Kanold PO, Micheva KD, Busse B, Shamloo M, Smith SJ, Shatz CJ
538 (2009) Classical MHCI molecules regulate retinogeniculate refinement and limit ocular
539 dominance plasticity. Neuron 64:463–470.

540 Davis GW (2013) Homeostatic signaling and the stabilization of neural function. Neuron 80:718–
541 728.

542 Deng W, Aimone JB, Gage FH (2010) New neurons and new memories: how does adult
543 hippocampal neurogenesis affect learning and memory? Nat Rev Neurosci 11:339–350.

544 Deshmukh SS, Knierim JJ (2011) Representation of non-spatial and spatial information in the
545 lateral entorhinal cortex. Front Behav Neurosci 5:69.

546 Dieni CV, Nietz AK, Panichi R, Wadiche JI, Overstreet-Wadiche L (2013) Distinct determinants
547 of sparse activation during granule cell maturation. J Neurosci 33:19131–19142.

548 Dieni CV, Panichi R, Aimone JB, Kuo CT, Wadiche JI, Overstreet-Wadiche L (2016) Low
549 excitatory innervation balances high intrinsic excitability of immature dentate neurons. Nat
550 Commun 7:11313.

551 Feldman DE (2009) Synaptic mechanisms for plasticity in neocortex. Annu Rev Neurosci 32:33–
552 55.

553 Ferbinteanu J, Holsinger RM, McDonald RJ (1999) Lesions of the medial or lateral perforant
554 path have different effects on hippocampal contributions to place learning and on fear
555 conditioning to context. Behav Brain Res 101:65–84.

556 Fortin DA, Tillo SE, Yang G, Rah J-C, Melander JB, Bai S, Soler-Cedeño O, Qin M, Zemelman
557 BV, Guo C, Mao T, Zhong H (2014) Live imaging of endogenous PSD-95 using ENABLED:
558 a conditional strategy to fluorescently label endogenous proteins. J Neurosci 34:16698–
559 16712.

560 Ge S, Goh ELK, Sailor KA, Kitabatake Y, Ming G-L, Song H (2006) GABA regulates synaptic
561 integration of newly generated neurons in the adult brain. Nature 439:589–593.

562 Ge S, Yang C-H, Hsu K-S, Ming G-L, Song H (2007) A critical period for enhanced synaptic
563 plasticity in newly generated neurons of the adult brain. Neuron 54:559–566.

564 Goodman CS, Shatz CJ (1993) Developmental mechanisms that generate precise patterns of
565 neuronal connectivity. Cell 72 Suppl:77–98.

566 Hafting T, Fyhn M, Molden S, Moser M-B, Moser EI (2005) Microstructure of a spatial map in
567 the entorhinal cortex. Nature 436:801–806.

568 Hargreaves EL, Rao G, Lee I, Knierim JJ (2005) Major dissociation between medial and lateral
569 entorhinal input to dorsal hippocampus. Science 308:1792–1794.

570 Harris KM, Jensen FE, Tsao B (1992) Three-dimensional structure of dendritic spines and
571 synapses in rat hippocampus (CA1) at postnatal day 15 and adult ages: implications for the
572 maturation of synaptic physiology and long-term potentiation [published erratum appears in
573 J Neurosci 1992 Aug; 12 (8): following table of contents]. Journal of Neuroscience
574 12:2685–2705.

575 Holtmaat A, Svoboda K (2009) Experience-dependent structural synaptic plasticity in the
576 mammalian brain. Nat Rev Neurosci 10:647–658.

577 Huang EJ, Reichardt LF (2001) Neurotrophins: roles in neuronal development and function.

578 Annu Rev Neurosci 24:677–736.

579 Hunsaker MR, Mooy GG, Swift JS, Kesner RP (2007) Dissociations of the medial and lateral
580 perforant path projections into dorsal DG, CA3, and CA1 for spatial and nonspatial (visual
581 object) information processing. Behav Neurosci 121:742–750.

582 Isaac JT, Nicoll RA, Malenka RC (1995) Evidence for silent synapses: implications for the
583 expression of LTP. Neuron 15:427–434.

584 Katz LC, Shatz CJ (1996) Synaptic activity and the construction of cortical circuits. Science
585 274:1133–1138.

586 Kee N, Teixeira CM, Wang AH, Frankland PW (2007) Preferential incorporation of adult-
587 generated granule cells into spatial memory networks in the dentate gyrus. Nat Neurosci
588 10:355–362.

589 Knierim JJ, Neunuebel JP, Deshmukh SS (2014) Functional correlates of the lateral and medial
590 entorhinal cortex: objects, path integration and local-global reference frames. Philos Trans
591 R Soc Lond B Biol Sci 369:20130369.

592 Knudsen EI (2004) Sensitive periods in the development of the brain and behavior. J Cogn
593 Neurosci 16:1412–1425.

594 Lepousez G, Nissant A, Lledo P-M (2015) Adult neurogenesis and the future of the rejuvenating
595 brain circuits. Neuron 86:387–401.

596 LeVay S, Wiesel TN, Hubel DH (1980) The development of ocular dominance columns in
597 normal and visually deprived monkeys. J Comp Neurol 191:1–51.

598 Lindvall O, Kokaia Z (2006) Stem cells for the treatment of neurological disorders. Nature
599 441:1094–1096.

600 Luikart BW, Schnell E, Washburn EK, Bensen AL, Tovar KR, Westbrook GL (2011) Pten
601 knockdown in vivo increases excitatory drive onto dentate granule cells. J Neurosci
602 31:4345–4354.

603 Magee JC (2000) Dendritic integration of excitatory synaptic input. Nat Rev Neurosci 1:181–
604 190.

605 Majewska AK, Sur M (2006) Plasticity and specificity of cortical processing networks. Trends
606 Neurosci 29:323–329.

607 Malenka RC, Bear MF (2004) LTP and LTD: an embarrassment of riches. Neuron 44:5–21.

608 Marín-Burgin A, Mongiat LA, Pardi MB, Schinder AF (2012) Unique processing during a period
609 of high excitation/inhibition balance in adult-born neurons. Science 335:1238–1242.

610 Mates SL, Lund JS (1983) Spine formation and maturation of type 1 synapses on spiny stellate
611 neurons in primate visual cortex. J Comp Neurol 221:91–97.

612 Miller M, Peters A (1981) Maturation of rat visual cortex. II. A combined Golgi-electron
613 microscope study of pyramidal neurons. J Comp Neurol 203:555–573.

614 Ming G-L, Song H (2011) Adult neurogenesis in the mammalian brain: significant answers and
615 significant questions. Neuron 70:687–702.

616 Nakashiba T, Cushman JD, Pelkey KA, Renaudineau S, Buhl DL, McHugh TJ, Rodriguez
617 Barrera V, Chittajallu R, Iwamoto KS, McBain CJ, Fanselow MS, Tonegawa S (2012)
618 Young dentate granule cells mediate pattern separation, whereas old granule cells facilitate
619 pattern completion. Cell 149:188–201.

620 Overstreet LS, Hentges ST, Bumaschny VF, de Souza FSJ, Smart JL, Santangelo AM, Low MJ,
621 Westbrook GL, Rubinstein M (2004) A transgenic marker for newly born granule cells in
622 dentate gyrus. J Neurosci 24:3251–3259.

623 Overstreet-Wadiche LS, Bensen AL, Westbrook GL (2006) Delayed development of adult-
624 generated granule cells in dentate gyrus. J Neurosci 26:2326–2334.

625 Overstreet-Wadiche LS, Westbrook GL (2006) Functional maturation of adult-generated granule
626 cells. Hippocampus 16:208–215.

627 Parent AS, Pinson A, Woods N, Chatzi C, Vaaga CE, Bensen A, Gérard A, Thome JP,
628 Bourguignon JP, Westbrook GL (2016) Early exposure to Aroclor 1254 in vivo disrupts the
629 functional synaptic development of newborn hippocampal granule cells. Eur J Neurosci
630 44:3001–3010.

631 Perederiy JV, Luikart BW, Washburn EK, Schnell E, Westbrook GL (2013) Neural injury alters
632 proliferation and integration of adult-generated neurons in the dentate gyrus. J Neurosci
633 33:4754–4767.

634 Rolls ET, Treves A, Rolls ET (1998) Neural networks and brain function. Available at:
635 http://www.oxcns.org/papers/Rolls%20Treves%201998%20Capacity%20of%20pattern%20
636 association%20networks.pdf.

637 Sahay A, Scobie KN, Hill AS, O'Carroll CM, Kheirbek MA, Burghardt NS, Fenton AA, Dranovsky
638 A, Hen R (2011) Increasing adult hippocampal neurogenesis is sufficient to improve pattern
639 separation. Nature 472:466–470.

640 Sando R, Bushong E, Zhu Y, Huang M, Considine C, Phan S, Ju S, Uytiepo M, Ellisman M,
641 Maximov A (2017) Assembly of Excitatory Synapses in the Absence of Glutamatergic
642 Neurotransmission. Neuron 94:312–321.e3.

643 Sato M, Stryker MP (2008) Distinctive features of adult ocular dominance plasticity. J Neurosci
644 28:10278–10286.

645 Saxe MD, Battaglia F, Wang J-W, Malleret G, David DJ, Monckton JE, Garcia ADR, Sofroniew
646 MV, Kandel ER, Santarelli L, Others (2006) Ablation of hippocampal neurogenesis impairs
647 contextual fear conditioning and synaptic plasticity in the dentate gyrus. Proceedings of the
648 National Academy of Sciences 103:17501–17506.

649 Schiavo G, Benfenati F, Poulain B, Rossetto O, Polverino de Laureto P, DasGupta BR,
650 Montecucco C (1992) Tetanus and botulinum-B neurotoxins block neurotransmitter release
651 by proteolytic cleavage of synaptobrevin. Nature 359:832–835.

652 Schmidt-Hieber C, Jonas P, Bischofberger J (2004) Enhanced synaptic plasticity in newly

653 generated granule cells of the adult hippocampus. Nature 429:184–187.

654 Tagawa Y, Kanold PO, Majdan M, Shatz CJ (2005) Multiple periods of functional ocular
655 dominance plasticity in mouse visual cortex. Nat Neurosci 8:380–388.

656 Toni N, Laplagne DA, Zhao C, Lombardi G, Ribak CE, Gage FH, Schinder AF (2008) Neurons
657 born in the adult dentate gyrus form functional synapses with target cells. Nat Neurosci
658 11:901–907.

659 Toni N, Teng EM, Bushong EA, Aimone JB, Zhao C, Consiglio A, van Praag H, Martone ME,
660 Ellisman MH, Gage FH (2007) Synapse formation on neurons born in the adult
661 hippocampus. Nat Neurosci 10:727–734.

662 Tovar KR, Maher BJ, Westbrook GL (2009) Direct actions of carbenoxolone on synaptic
663 transmission and neuronal membrane properties. J Neurophysiol 102:974–978.

664 Tronel S, Belnoue L, Grosjean N, Revest J-M, Piazza P-V, Koehl M, Abrous DN (2012) Adult-
665 born neurons are necessary for extended contextual discrimination. Hippocampus 22:292–
666 298.

667 Tsao A, Moser M-B, Moser EI (2013) Traces of experience in the lateral entorhinal cortex. Curr
668 Biol 23:399–405.

669 Van Cauter T, Camon J, Alvernhe A, Elduayen C, Sargolini F, Save E (2013) Distinct roles of
670 medial and lateral entorhinal cortex in spatial cognition. Cereb Cortex 23:451–459.

671 van Praag H, Schinder AF, Christie BR, Toni N, Palmer TD, Gage FH (2002) Functional
672 neurogenesis in the adult hippocampus. Nature 415:1030–1034.

673 Vivar C, Potter MC, Choi J, Lee J-Y, Stringer TP, Callaway EM, Gage FH, Suh H, van Praag H
674 (2012) Monosynaptic inputs to new neurons in the dentate gyrus. Nat Commun 3:1107.

675 Walsh MK, Lichtman JW (2003) In vivo time-lapse imaging of synaptic takeover associated with
676 naturally occurring synapse elimination. Neuron 37:67–73.

677 Witter MP (2007) The perforant path: projections from the entorhinal cortex to the dentate gyrus.
678 Prog Brain Res 163:43–61.

679 Yasuda M, Mayford MR (2006) CaMKII activation in the entorhinal cortex disrupts previously
680 encoded spatial memory. Neuron 50:309–318.

681 Yoganarasimha D, Rao G, Knierim JJ (2011) Lateral entorhinal neurons are not spatially
682 selective in cue-rich environments. Hippocampus 21:1363–1374.

683 Yuste R, Bonhoeffer T (2004) Genesis of dendritic spines: insights from ultrastructural and
684 imaging studies. Nat Rev Neurosci 5:24–34.

685 Zhao C, Teng EM, Summers RG Jr, Ming G-L, Gage FH (2006) Distinct morphological stages of
686 dentate granule neuron maturation in the adult mouse hippocampus. J Neurosci 26:3–11.

687 Ziv NE, Garner CC (2001) Principles of glutamatergic synapse formation: seeing the forest for
688 the trees. Curr Opin Neurobiol 11:536–543.

689 **Figure Legends:**

690

691 **Figure 1: Laminar specific electrical and optical stimulation**. (A) Circuit schematic
692 demonstrating laminar specific input from medial entorhinal cortex (MEC) and lateral entorhinal
693 cortex (LEC). Within the molecular layer of the dentate gyrus, MEC axons reside in the middle
694 molecular layer (MML) whereas lateral entorhinal cortex axons reside in the outer molecular
695 layer (OML). (B) Demonstration of laminar specific input using field EPSP recordings. When the
696 field recording electrode and bipolar electrode are within the same layer, a current sink is
697 observed as a negative voltage deflection. A current source can be observed when the field
698 electrode and bipolar electrode are in adjacent layers. (C) Laminar specific expression of ChR2
699 following viral injection into the medial entorhinal cortex (left) or lateral entorhinal cortex (right).
700 Scale bar: 100 μm. (D) Comparison of lamina-specific optogenetic stimulation in mature (black)
701 and newborn cells (green). (E) Comparison of the strength of the maximal light evoked EPSCs
702 from each lamina in mature and newborn (p21) granule cells.

703

704 **Figure 2: Synaptic maturation and development** (A) Spine density measurements in MML
705 (top) and OML (bottom) at 3 and 6 week old dentate granule cells. Scale bar: 5 μm. (B)
706 Developmental increase in spine density across cell development in middle molecular layer
707 (black) and outer molecular layer (red). *Inset*: Average spine density across layers increases
708 between 3 and 4 weeks post-mitosis, then remains constant between 4 and 12 weeks. (C)
709 Developmental increase in the percentage of spines with filopodial morphology in both MML
710 (black) and OML (red). (D) Miniature EPSC recordings in the presence of 10 μM SR95531 and
711 1 μM TTX to isolate excitatory events. mEPSCs were recorded at 3 and 6 weeks post mitosis.
712 (E) There was no difference in the miniature EPSC frequency at 3 and 6 weeks post mitosis. (F)
713 There was a significant decrease in miniature EPSC amplitude, suggesting weaker synaptic
714 inputs at 6 weeks post-mitosis.

715

716 **Figure 3: Silencing synaptic input with Tetanus toxin expression** (A) Comparison of
717 synaptic responses in autaptically cultured neurons in control (left) and following tetanus toxin
718 infection (TeNT). (B) Expression of TeNT completely abolishes synaptic responses in
719 autaptically cultured neurons. (C) Schematic of TeNT viral injection into the medial entorhinal
720 cortex, which will functionally silence axons in the middle molecular layer of the dentate gyrus.
721 (D) Expression of TeNT in the middle molecular layer dramatically reduces the intensity of
722 VGluT1 expression in the middle molecular layer, indicating a disruption of presynaptic function.

723 Scale bar: 100 μm. (E) TeNT expression did not elicit astrogliosis. (F, G) Electron micrographs
724 from control (F) and TeNT overexpressing (G) axons. TeNT expression results in axonal
725 swelling and vesicle accumulation (b=axonal bouton, s=dendritic spine, arrowheads=synapse).
726 Scale bar: 500 nm. (H) Field EPSP recordings from the middle molecular layer while electrically
727 stimulating the medial perforant path fibers. (I) fEPSP responses were significantly attenuated
728 when TeNT was expressed in the MML, without changing fiber volley amplitudes.
729
730 **Figure 4: Silencing the middle molecular layer impairs normal synaptic innervation in the**
731 **outer molecular layer.** (A) Expression of ChR2 in the outer molecular layer, with TeNT
732 expression in the middle molecular layer (MML:TeNT). Scale bar: 100 μm. (B) Comparison of
733 synaptic responses in mature neurons (top) and newborn neurons (bottom) in control and
734 MML:TeNT conditions. (C) TeNT expression in the MML significantly reduces the amplitude of
735 OML-evoked responses selectively in newborn cells. (D) MML:TeNT expression increases the
736 paired pulse ratio of OML axons, selectively in newborn cells. (E) Retroviral labeling of newborn
737 dentate granule cells in control (left) and with MML:TeNT (right). Scale bar: 35 μm. (F, G) Spine
738 density is significantly reduced in both MML and OML following MML:TeNT expression. Scale
739 bar in (F): 2.5 μm.
740

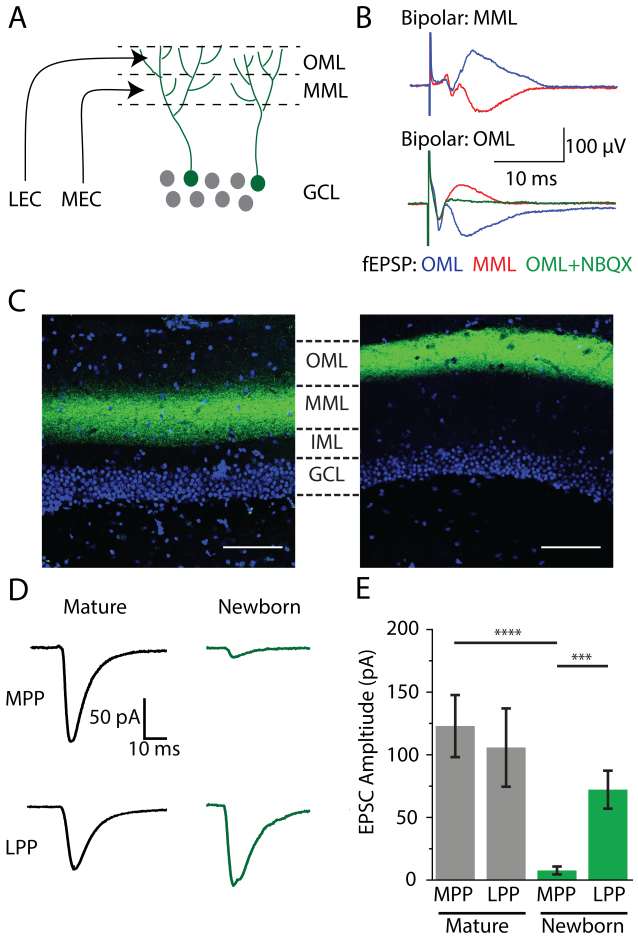
A
OML
MML
LEC
MEC
GCL
B
Bipolar: MML
Bipolar: OML
100 µV
10 ms
fEPSP: OML MML OML+NBQX
C
OML
MML
IML
GCL
D
Mature
Newborn
MPP
50 pA
10 ms
LPP
E
EPSC Amplitude (pA)
200
150
100
50
0
****
***
MPP LPP MPP LPP
Mature
Newborn

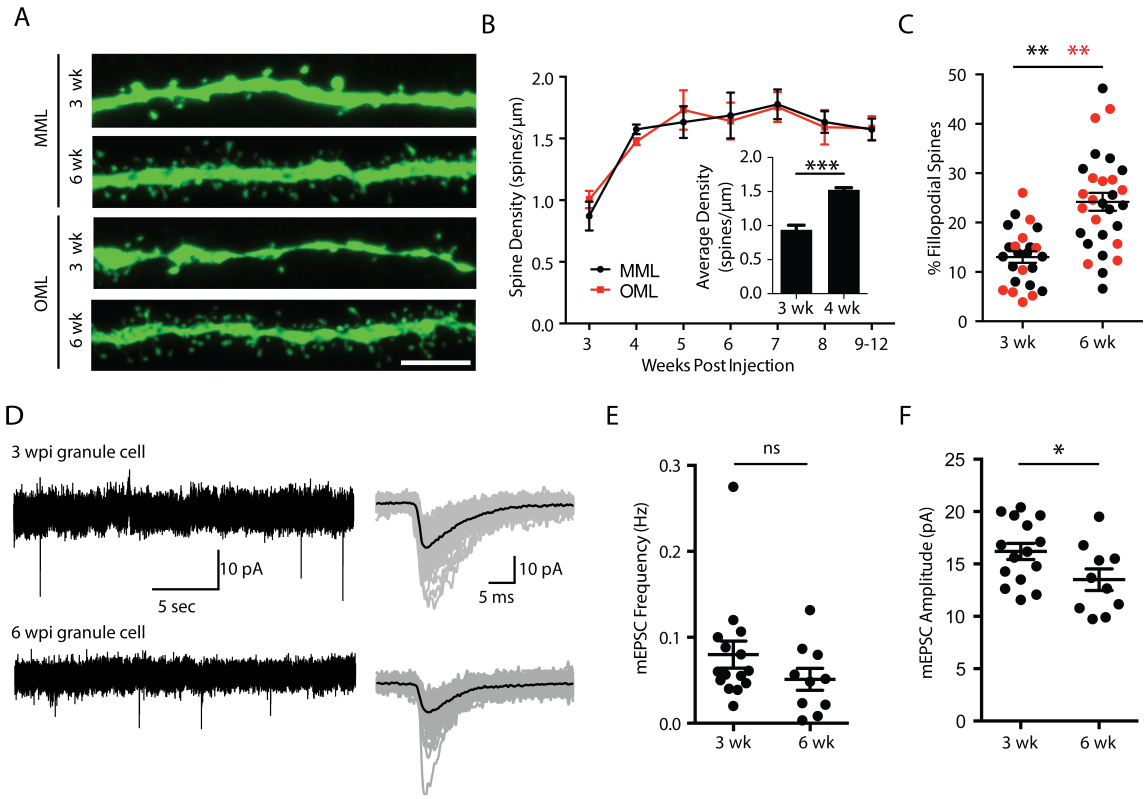
A
MML
3 wk
6 wk
OML
3 wk
6 wk
B
Spine Density (spines/µm)
2.0
1.5
1.0
0.5
0.0
MML
OML
Average Density (spines/µm)
***
3 wk
4 wk
3
4
5
6
7
8
9-12
Weeks Post Injection
C
**
**
% Fillopodial Spines
50
40
30
20
10
0
3 wk
6 wk
D
3 wpi granule cell
10 pA
5 sec
10 pA
5 ms
6 wpi granule cell
E
ns
mEPSC Frequency (Hz)
0.3
0.2
0.1
0.0
3 wk
6 wk
F
*
mEPSC Amplitude (pA)
25
20
15
10
5
0
3 wk
6 wk

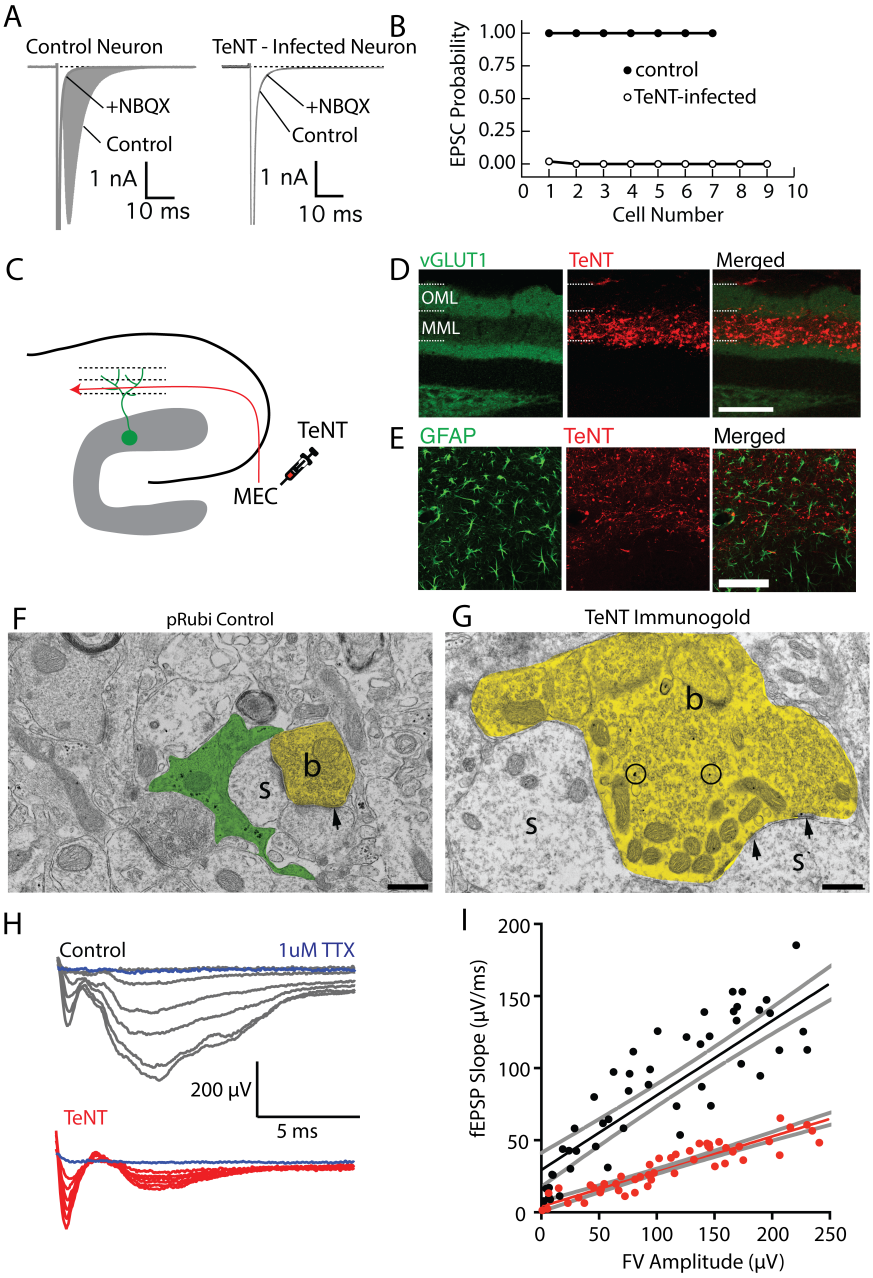
A
Control Neuron
TeNT - Infected Neuron
+NBQX
Control
1 nA
10 ms
B
EPSC Probability
1.00
0.75
0.50
0.25
0.00
control
TeNT-infected
0 1 2 3 4 5 6 7 8 9 10
Cell Number
C
TeNT
MEC
D
vGLUT1
TeNT
Merged
OML
MML
E
GFAP
TeNT
Merged
F
pRubi Control
b
s
G
TeNT Immunogold
b
s
s
H
Control
1uM TTX
200 µV
5 ms
TeNT
I
fEPSP Slope (µV/ms)
200
150
100
50
0
0 50 100 150 200 250
FV Amplitude (µV)

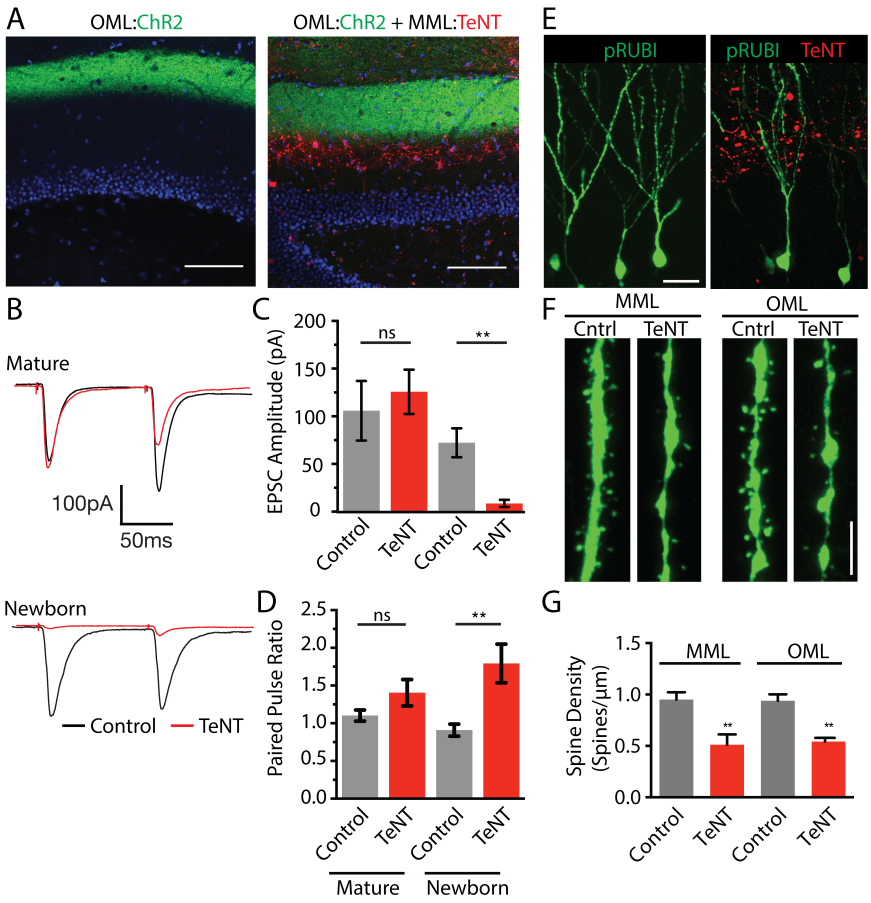
A
OML:ChR2
OML:ChR2 + MML:TeNT
E
pRUBI
pRUBI TeNT
B
Mature
100pA
50ms
Newborn
Control
TeNT
C
EPSC Amplitude (pA)
200
150
100
50
0
ns
**
Control
TeNT
Control
TeNT
F
MML
OML
Cntrl
TeNT
Cntrl
TeNT
D
Paired Pulse Ratio
2.5
2.0
1.5
1.0
0.5
0.0
ns
**
Control
TeNT
Control
TeNT
Mature
Newborn
G
Spine Density (Spines/µm)
1.5
1.0
0.5
0.0
MML
OML
**
**
Control
TeNT
Control
TeNT